ChemPubSoc Europe

DOI: 10.1002/chem.201901157

CHEMISTRY A European Journal Communication

Contrast Agents |*Hot Paper*|

High-Field Detection of Biomarkers with Fast Field-Cycling MRI: The Example of Zinc Sensing

Markus Bödenler,[a] Kyangwi P. Malikidogo,[b] Jean-François Morfin,[b] Christoph Stefan Aigner,[a] Éva Tóth,[b] Célia S. Bonnet,*[b] and Hermann Scharfetter*[a]

Abstract: Many smart magnetic resonance imaging (MRI) probes provide response to a biomarker based on modulation of their rotational correlation time. The magnitude of such MRI signal changes is highly dependent on the magnetic field and the response decreases dramatically at high fields (>2 T). To overcome the loss of efficiency of responsive probes at high field, with fast-field cycling magnetic resonance imaging (FFC-MRI) we exploit field-dependent information rather than the absolute difference in the relaxation rate measured in the absence and in the presence of the biomarker at a given imaging field. We report here the application of fast field-cycling techniques combined with the use of a molecular probe for the detection of Zn^{2+} to achieve 166% MRI signal enhancement at 3 T, whereas the same agent provides no detectable response using conventional MRI. This approach can be generalized to any biomarker provided the detection is based on variation of the rotational motion of the probe.

Magnetic resonance imaging (MRI) is a prevalent diagnostic technique in medicine, due to its high temporal and spatial resolution, penetration depth, superb soft tissue contrast, and the lack of harmful ionizing radiation. Contrast in MRI is essentially obtained by differences in local proton density and spatially varying relaxation times in the tissue of interest. MRI has moderate sensitivity compared to nuclear or optical imaging and therefore requires, in certain cases, amplification strategies to enhance water proton relaxation, such as the use of a contrast agent. MRI has great potential for molecular imaging (MI), which can provide spatially and temporally resolved maps of biomarkers (pH, presence of cations, enzymes, metabolites, temperature, etc.) to unravel molecular processes in tissues rather than their simple morphology. MI might enable earlier diagnosis, as these physiological changes happen prior to the morphological changes typically monitored by traditional MRI. MI requires the use of a contrast agent selective to the biomarker to detect.

The majority of MRI contrast agents are Gd^{3+} complexes, which affect mainly the longitudinal relaxation time T_1. Their efficiency, called relaxivity r_1, is defined by the paramagnetic relaxation rate enhancement of water protons by concentration unit of the agent. Two main approaches exist to render Gd^{3+} complexes responsive to the presence of a biomarker: altering either the number of water molecules directly coordinated to Gd^{3+}, q, or the rotational correlation time, τ_R, of the complex.[1] With the "q-activated" approach, the response is roughly constant at any magnetic field, whereas with the "τ_R-activated" approach (τ_R modulation), the response is highly field-dependent. The effect of τ_R on relaxivity is reflected in the characteristic shape of the ^1H nuclear magnetic relaxation dispersion (NMRD) profile of slowly tumbling systems and provides the best efficiency at intermediate fields (relaxivity peak between 0.5–1.5 T).[2] At higher magnetic fields (3 T and above), where the resolution of MRI is better, the benefit of long τ_R on proton relaxivity is diminished.

Fast field-cycling magnetic resonance imaging (FFC-MRI) is a novel strategy in MRI that takes specific advantage of the magnetic field dependency of relaxivity. In contrast to conventional MRI where the main magnetic field is fixed, in FFC-MRI the magnetic field can be altered during the imaging sequence.[3] This allows for exploiting field-dependent information based on the partial derivative of the longitudinal relaxation rate with respect to the magnetic field, dR_1/dB_0. This method is particularly interesting to visualize slowly tumbling agents with high R_1 dispersion (i.e., high dR_1/dB_0; $R_1 = 1/T_1$ and $r_1 = (R_1 - R_{1dia})/[Gd]$, where R_{1dia} is the diamagnetic contribution to the relaxation rate and [Gd] is the concentration of the contrast agent). It was successfully used to image probes that exhibit a strong relaxivity response upon protein binding, especially in the case of human serum albumin (HSA).[4] To the best of our knowledge, this technique has not been used for responsive contrast agents. We demonstrate here its potential in zinc detection.

Zinc plays a pivotal role in various cellular processes including enzyme activities, DNA and protein synthesis or signal transduction.[5] Misregulations in Zn^{2+} homeostasis are associ-

[a] *M. Bödenler, Dr. C. S. Aigner, Dr. H. Scharfetter*
Institute of Medical Engineering
Graz University of Technology, Graz (Austria)
E-mail: hermann.scharfetter@tugraz.at

[b] *Dr. K. P. Malikidogo, Dr. J.-F. Morfin, Dr. É. Tóth, Dr. C. S. Bonnet*
Centre de Biophysique Moléculaire, CNRS
Rue Charles Sadron, 45071 Orléans Cedex 2 (France)
E-mail: celia.bonnet@cnrs.fr

Supporting information, which includes full experimental details, and the ORCID identification number(s) for the author(s) of this article can be found under: https://doi.org/10.1002/chem.201901157.

ated with diabetes,[6] cancers,[7] and neurodegenerative diseases.[8] Significant effort has been devoted to non-invasive imaging of Zn^{2+} distribution to study its role in biological processes and to improve early stage diagnosis of diseases. Zn^{2+}-responsive probes have been designed based on q or τ_R modulation.[9] The rotational correlation time is typically controlled through binding of the Gd^{3+} complex to a macromolecule or protein, which becomes more important after Zn^{2+} coordination (Figure 1). This approach was mostly investigated for HSA

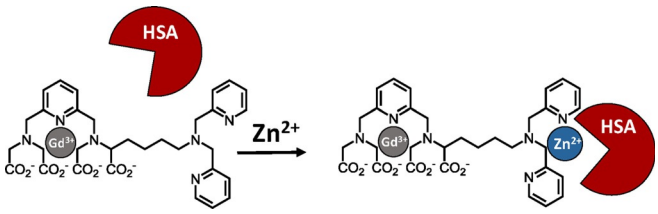

Figure 1. Chemical structure of the contrast agent and schematic representation of Zn^{2+} detection mechanism, based on τ_R modulation due to increased binding affinity in the presence of Zn^{2+}.

because of its high concentration (0.6 mM) and the presence of several binding sites at the surface of the protein.[10] Although the relaxivity response to Zn^{2+} is remarkable at intermediate fields with these systems, it decreases dramatically at high fields.[1a] q-activated contrast agents could represent an efficient way to obtain a maximal response at higher fields, but their rational design remains a difficult challenge especially for metal ion detection. Indeed, the coordination spheres of both Gd^{3+} and the cation to detect, as well as the flexibility and length of the linker between the Gd^{3+}- and the Zn^{2+}-coordinating units should be all controlled in the design.[9] Therefore, novel strategies allowing sensitive, high-field MRI detection of τ_R-activated responsive probes are highly desirable.

Herein, we report on using FFC-MRI with a τ_R-activated, Zn^{2+} responsive agent in the presence of HSA. FFC-MRI takes benefit of the change of dR_1/dB_0 (slope in the NMRD profile), rather than the absolute difference in $R_1 = 1/T_1$ at a fixed magnetic field, upon Zn^{2+} binding. In a proof-of-concept in vitro experiment, we demonstrate that it is possible to overcome the loss of efficiency at a clinically relevant field strength and to generate Zn^{2+} dependent image contrast. Indeed, though the agent does not respond to Zn^{2+} in classical MRI at 3 T, 166% MRI intensity increase is achieved upon Zn^{2+}-binding in FFC-MRI at the same field.

Our Zn^{2+}-responsive probe, GdL, comprises three moieties: (1) a Gd^{3+}-complexing unit based on a pyridine backbone; (2) a bis(pyridinylmethyl)amine (DPA) for Zn^{2+} chelation; and (3) a linker (Figure 1). The pyridinic backbone has shown to possess relatively good thermodynamic stability and kinetic inertness, which previously enabled its safe application in animal studies.[11] In this complex, Gd^{3+} has two inner sphere water molecules, which are not replaced by physiological anions, and result in a high relaxivity. DPA displays good affinity ($K_d = 7.57$) and sufficient selectivity[12] for Zn^{2+}, and has been previously used for the detection of Zn^{2+} by MRI.[13]

The hydrophobic moieties of the Gd^{3+} complex promote interaction with HSA, which generate a field-dependent relaxometric response to Zn^{2+} at physiological HSA concentration as illustrated in Figure 2. The NMRD profiles, both in the presence and in the absence of Zn^{2+}, show the hump typical for macromolecular systems at intermediate fields. The Zn^{2+} response is maximal at 0.7–1 T with a relaxivity increase of about 25% upon Zn^{2+}-binding. In contrast, at 9.4 T, a roughly 30% relaxivity decrease is obtained, while around 3 T, the response vanishes as the two NMRD profiles cross each other. In accordance with these results, no visible difference in R_1 can be observed in response to increasing Zn^{2+} concentration in solutions of GdL and HSA, by using standard MRI methods at 3 T (Figure 3 b).

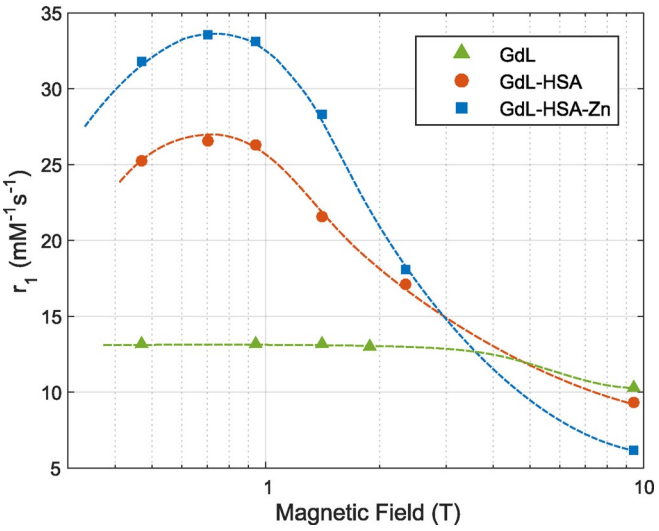

Figure 2. ^{1}H NMRD profiles of GdL alone (1.35 mM), GdL (0.26 mM) and GdL-Zn (equimolar ratio; 0.27 mM) in the presence of 0.6 mM of HSA at pH 7.4 (HEPES buffer) and 298 K; the symbols represent measured points and the dashed lines serve to guide the eye.

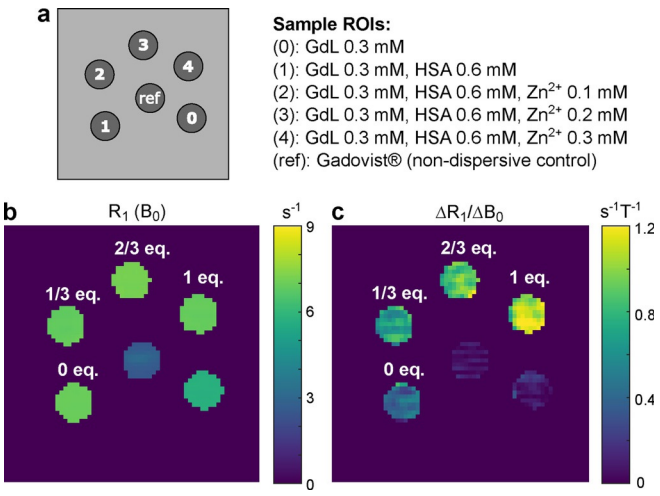

Figure 3. (a) Sample arrangement for the MR phantom measurements. (b) R_1 map obtained at the nominal B_0 field strength (2.89 T) of the MRI system. No visible difference in R_1 can be observed upon the addition of Zn^{2+}. (c) $\Delta R_1/\Delta B_0$ map calculated by subtracting R_1 maps for 2.99 and 2.79 T. The high contrast for samples with increasing Zn^{2+} concentration should be noted. See the SI for image acquisition details.

For FFC-MRI, the hardware was realized by means of an additional B_0 insert coil synchronized with a clinical MRI system with a main magnetic field strength B_0 of 2.89 T.[14] The field-cycling hardware is capable of generating offset fields ΔB_0 of $\pm$100 mT within a minimum ramp time of 1 ms. Images were acquired at three different evolution fields (2.79, 2.89, and 2.99 T) using a saturation prepared spin echo sequence, where B_0 was ramped to the desired field-shift for a duration T_{evol} between the preparation pulse and image acquisition. A detailed description of the imaging experiments and the analysis of the regions of interest (ROI) is given in the Supporting Information (SI).

R_1 maps were obtained at 2.89 T (the nominal B_0 field strength of the MRI system; Figure 3b), 2.79 T (Figure S1c), and 2.99 T (Figure S1d) by cycling the evolution field. The magnetic field dependence was calculated from the difference between R_1 maps for 2.99 T and 2.79 T. After normalization with ΔB_0, this yields the R_1 dispersion map presented in Figure 3c (i.e., $\Delta R_1/\Delta B_0$ within the achievable field-cycling range). No significant $\Delta R_1/\Delta B_0$ is visible for the reference samples containing Gadovist[15] and GdL without HSA as expected from the NMRD profile. The complex without Zn^{2+} in the presence of HSA shows a background dispersion due to the formation of the GdL-HSA adduct as shown in the NMRD profile (Figure 2). It represents the "inactivated" state of the probe. The FFC-MRI signal intensity increases with increasing Zn^{2+} concentration up to one equivalent of Zn^{2+} (Figure 3c; see Table S1 in the SI for values). Figure 4 (and Table S1, SI) summarizes the relative signal enhancement upon Zn^{2+} addition to the GdL/HSA solution. The maximum signal enhancement is about 166% upon the addition of 1 equivalent of Zn^{2+}, in contrast to no signal enhancement detected with standard MRI at the nominal field strength of 2.89 T. This is quite remarkable because, even at the most optimal field (0.5 T), the relaxivity change upon Zn^{2+}-binding is only 26% for this probe (see NMRD profile). For comparison, 100 to 220% relaxivity changes were reported for *q*-activated Zn-responsive contrast agents.[16] Similar relaxivity response (165%) was obtained for the most-studied τ_R-activated contrast agent at 0.5 T;[13c] however, at higher field the response decreases dramatically. This last agent was used in vivo to detect Zn^{2+} in the pancreas[17] or in prostate cancer.[18] These studies were performed at 9.4 T, where relaxometric data predict about 50% relaxivity response to Zn^{2+}. In a recent study, Zn^{2+} was imaged with another contrast agent providing a relaxivity response of only 7.5% at the imaging field of 9.4 T.[19] With the FFC-MRI technique, remarkably higher signal variations are achieved. Moreover, the $\Delta R_1/\Delta B_0$ signal increase is linearly proportional to Zn^{2+} concentration (see the SI for linear regression analysis). This, combined with our previously reported bimodal quantification approach,[20] might open unprecedented opportunities towards high precision zinc quantification.

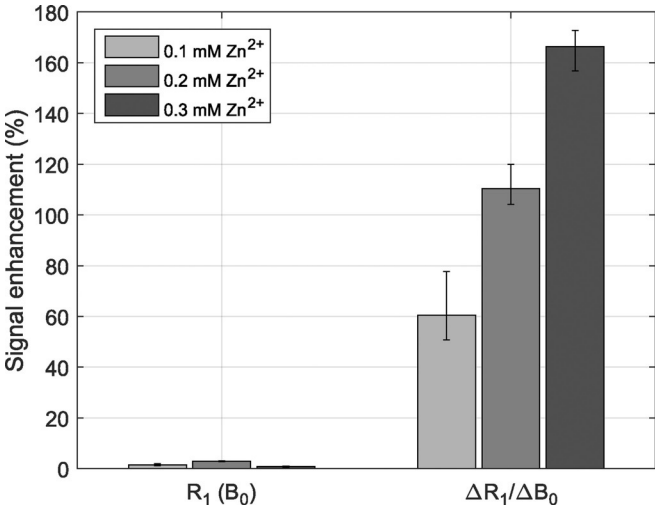

Figure 4. Percent signal enhancement of the Zn^{2+} response for a change in R_1 at the nominal B_0 of the MRI system (left) and the change of $\Delta R_1/\Delta B_0$ accessed by FFC-MRI (right). The signal enhancement was calculated with respect to the value obtained for the GdL-HSA complex without Zn^{2+}; data is presented in 1st quartile, median, and 3rd quartile. The activation response is linear with respect to an increasing Zn^{2+} concentration (up to 1 equiv Zn^{2+}); see the SI for the linear regression analysis.

In the magnetic field range of 1.5 T to 3 T, routinely used for clinical imaging, the R_1 dispersion of tissues is inherently weak. For contrast agents exhibiting a large $\Delta R_1/\Delta B_0$, this small tissue R_1 dispersion (e.g., $-0.19\ s^{-1}T^{-1}$ for murine muscle tissue at 1.5 T) represents a negligible anatomical background signal.[21] In our example, if any free (not protein-bound) GdL or GdL-Zn is present, it will be "silent" (see Figure 3c), as the NMRD curves of such small complexes show no dispersion at these fields. On the other hand, the binding of GdL to HSA in the absence of Zn^{2+} entails a dispersion (background signal) that cannot be suppressed in the FFC-MR image. In order to decrease this signal of the inactivated state and to generate an even more important response to Zn^{2+}, the affinity of the GdL probe for HSA could be decreased.

It is important to estimate the in vivo detection limit of zinc. Considering the linear response of $\Delta R_1/\Delta B_0$ to zinc concentration and assuming that the background signal is provided by the GdL-HSA adduct, a rough estimate of the detection limit would be 60 μM Zn^{2+} (corresponding to $\approx$0.2 equiv Zn^{2+} for 0.3 mM GdL concentration; see the SI for details). The contrast agent concentration used in this proof-of-principle study lies in the clinically relevant region (the approved dose ranges from 0.1 to 0.3 mmol kg^{-1});[22] and the estimated Zn^{2+} detection limit matches physiological concentrations which attain 100 μM to 1 mM in pancreatic regions or neurons.[23] It should be noted that FFC-MRI requires an insert coil to vary the B_0 field which, with respect to classical MRI, implies technical constraints on image acquisition, such as duty cycle considerations for electromagnetic operation, prolonged scan times and limited imaging region.[3b] Despite these constraints, pre-clinical FFC-MRI studies have been promising and show the feasibility of in vivo visualization of MRI probes with a detection limit of $\approx$40 μM.[3c,4b,c,21] This is rather encouraging as it suggests that the contrast agent concentration used in our study can be reduced which implies an even lower Zn^{2+} detection limit. Additional technical improvements and post-processing methods such as image denoising can further contribute to better detection limits, which will be subject of future investigations.

To conclude, we have demonstrated successful Zn^{2+} detection at 3 T using FFC-MRI (166% intensity increase), whereas no detection was possible with the same probe at this field using conventional MRI. As the chemical design of efficient Zn^{2+} responsive probes adapted to classical T_1 detection at high fields remains a challenge, FFC-MRI represents a highly interesting alternative. It can potentially add value to a great number of previously reported responsive probes that did not produce a detectable signal change at high fields. This technique is not solely limited to the detection of zinc, but can be adapted for the detection of any biomarker.

Acknowledgements

We thank Prof. Lothar Helm for the use of the Bruker Minispec relaxometer, and Agnès Pallier for performing ICP and some relaxivity measurements. This work was carried out within the frame of the COST Action CA15209 "European Network on NMR Relaxometry", supported by COST (European Cooperation in Science and Technology). M.B. and H.S. acknowledge the financial support by the European Commission in the framework of the H2020 Programme (FET-open) under grant agreement 665172, project "CONQUER". C.S.B. thanks the support of the French National Agency (grant ANR-13-JS07-0007).

Conflict of interest

The authors declare no conflict of interest.

Keywords: contrast agents · fast field-cycling · high-field detection · magnetic resonance imaging · molecular imaging

[1] a) V. C. Pierre, S. M. Harris, S. L. Pailloux, *Acc. Chem. Res.* **2018**, *51*, 342 – 351; b) C. S. Bonnet, E. Toth, in *Advances in Inorganic Chemistry, Vol 68: Insights from Imaging in Bioinorganic Chemistry* (Eds.: R. VanEldik, C. D. Hubbard), **2016**, pp. 43 – 96.

[2] S. Aime, M. Botta, D. Esteban-Gómez, C. Platas-Iglesias, *Mol. Phys.* **2019**, *117*, 898 – 909.

[3] a) D. J. Lurie, S. Aime, S. Baroni, N. A. Booth, L. M. Broche, C.-H. Choi, G. R. Davies, S. Ismail, D. O. Hogain, K. J. Pine, *C. R. Phys.* **2010**, *11*, 136 – 148; b) M. Bödenler, L. de Rochefort, P. J. Ross, N. Chanet, G. Guillot, G. R. Davies, C. Gösweiner, H. Scharfetter, D. J. Lurie, L. M. Broche, *Mol. Phys.* **2019**, *117*, 832 – 848; c) U. C. Hoelscher, S. Lother, F. Fidler, M. Blaimer, P. Jakob, *Magn. Reson. Mater. Phys. Biol. Med.* **2012**, *25*, 223 – 231.

[4] a) J. K. Alford, B. K. Rutt, T. J. Scholl, W. B. Handler, B. A. Chronik, *Magn. Reson. Med.* **2009**, *61*, 796 – 802; b) J. K. Alford, C. T. Farrar, Y. Yang, W. B. Handler, B. A. Chronik, T. J. Scholl, G. Madan, P. Caravan, *Proc. Intl. Soc. Mag. Reson. Med.* **2011**, *19*, 318; c) J. K. Alford, A. G. Sorensen, T. Brenner, B. A. Chronik, W. B. Handler, T. J. Scholl, G. Madan, P. Caravan, *Proc. Intl. Soc. Mag. Reson. Med.* **2011**, *19*, 452.

[5] W. Maret, *Adv. Nutr. Res.* **2013**, *4*, 82 – 91.

[6] N. Wijesekara, F. Chimienti, M. B. Wheeler, *Diabetes Obes. Metab.* **2009**, *11*, 202 – 214.

[7] C. Hogstrand, P. Kille, R. I. Nicholson, K. M. Taylor, *Trends Mol. Med.* **2009**, *15*, 101 – 111.

[8] G. Lyubartseva, J. L. Smith, W. R. Markesbery, M. A. Lovell, *Brain Pathol.* **2010**, *20*, 343 – 350.

[9] C. S. Bonnet, *Coord. Chem. Rev.* **2018**, *369*, 91 – 104.

[10] S. Aime, M. Botta, M. Fasano, S. G. Crich, E. Terreno, *J. Biol. Inorg. Chem.* **1996**, *1*, 312 – 319.

[11] C. S. Bonnet, F. Buron, F. Caille, C. M. Shade, B. Drahos, L. Pellegatti, J. Zhang, S. Villette, L. Helm, C. Pichon, F. Suzenet, S. Petoud, E. Toth, *Chem. Eur. J.* **2012**, *18*, 1419 – 1431.

[12] J. K. Romary, J. D. Barger, J. E. Bunds, *Inorg. Chem.* **1968**, *7*, 1142 – 1145.

[13] a) K. Hanaoka, K. Kikuchi, Y. Urano, T. Nagano, *J. Chem. Soc. Perkin Trans. 1* **2001**, 1840 – 1843; b) C. Rivas, G. J. Stasiuk, M. Sae-Heng, N. J. Long, *Dalton Trans.* **2015**, *44*, 4976 – 4985; c) A. C. Esqueda, J. A. Lopez, G. Andreu-De-Riquer, J. C. Alvarado-Monzon, J. Ratnakar, A. J. M. Lubag, A. D. Sherry, L. M. De Leon-Rodriguez, *J. Am. Chem. Soc.* **2009**, *131*, 11387 – 11391; d) J. Yu, A. F. Martins, C. Preihs, V. Clavijo Jordan, S. Chirayil, P. Zhao, Y. Wu, K. Nasr, G. E. Kiefer, A. D. Sherry, *J. Am. Chem. Soc.* **2015**, *137*, 14173 – 14179.

[14] M. Bödenler, M. Basini, M. F. Casula, E. Umut, C. Goesweiner, A. Petrovic, D. Kruk, H. Scharfetter, *J. Magn. Reson.* **2018**, *290*, 68 – 75.

[15] M. Rohrer, H. Bauer, J. Mintorovitch, M. Requardt, H. J. Weinmann, *Invest. Radiol.* **2005**, *40*, 715 – 724.

[16] a) L. M. Matosziuk, J. H. Leibowitz, M. C. Heffern, K. W. MacRenaris, M. A. Ratner, T. J. Meade, *Inorg. Chem.* **2013**, *52*, 12250 – 12261; b) M. Regueiro-Figueroa, S. Guenduez, V. Patinec, N. K. Logothetis, D. Esteban-Gomez, R. Tripier, G. Angelovski, C. Platas-Iglesias, *Inorg. Chem.* **2015**, *54*, 10342 – 10350.

[17] A. J. M. Lubag, L. M. De Leon-Rodriguez, S. C. Burgess, A. D. Sherry, *Proc. Natl. Acad. Sci. USA* **2011**, *108*, 18400 – 18405.

[18] M. V. Clavijo Jordan, S.-T. Lo, S. Chen, C. Preihs, S. Chirayil, S. Zhang, P. Kapur, W.-H. Li, L. M. De Leon-Rodriguez, A. J. M. Lubag, N. M. Rofsky, A. D. Sherry, *Proc. Natl. Acad. Sci. USA* **2016**, *113*, E5464 – E5471.

[19] A. F. Martins, V. C. Jordan, F. Bochner, S. Chirayil, N. Paranawithana, S. Zhang, S.-T. Lo, X. Wen, P. Zhao, M. Neeman, A. D. Sherry, *J. Am. Chem. Soc.* **2018**, *140*, 17456 – 17464.

[20] K. P. Malikidogo, I. Da Silva, J.-F. Morfin, S. Lacerda, L. Barantin, T. Sauvage, J. Sobilo, S. Lerondel, E. Toth, C. S. Bonnet, *Chem. Commun.* **2018**, *54*, 7597 – 7600.

[21] Y. T. Araya, F. Martinez-Santiesteban, W. B. Handler, C. T. Harris, B. A. Chronik, T. J. Scholl, *NMR Biomed.* **2017**, *30*, e3789.

[22] J. Wahsner, E. M. Gale, A. Rodriguez-Rodriguez, P. Caravan, *Chem. Rev.* **2019**, *119*, 957 – 1057.

[23] L. De Leon-Rodriguez, A. J. M. Lubag, A. D. Sherry, *Inorg. Chim. Acta* **2012**, *393*, 12 – 23.

Manuscript received: March 12, 2019
Revised manuscript received: April 12, 2019
Accepted manuscript online: April 16, 2019
Version of record online: May 21, 2019

